AIP Advances

Modeling interfacial mass transfer driven bubble growth in supersaturated solutions

Cite as: AIP Advances **10**, 105024 (2020); https://doi.org/10.1063/5.0020210
Submitted: 29 June 2020 . Accepted: 26 September 2020 . Published Online: 15 October 2020

Kurian J. Vachaparambil, and Kristian Etienne Einarsrud

Modeling interfacial mass transfer driven bubble growth in supersaturated solutions

Cite as: AIP Advances 10, 105024 (2020); doi: 10.1063/5.0020210
Submitted: 29 June 2020 • Accepted: 26 September 2020 •
Published Online: 15 October 2020

Kurian J. Vachaparambil[a] and Kristian Etienne Einarsrud[b]

AFFILIATIONS

Department of Materials Science and Engineering, Norwegian University of Science and Technology (NTNU), Trondheim 7491, Norway

[a]Author to whom correspondence should be addressed: kurian.j.vachaparambil@ntnu.no and kurian_jomy@hotmail.com
[b]Electronic mail: kristian.e.einarsrud@ntnu.no

ABSTRACT

A commonly encountered phenomenon in chemical processes is bubble evolution driven by supersaturation. On the continuum scale, this essentially involves interfacial mass transfer resulting in the growth of bubbles and their subsequent detachment from a surface. Analytical approaches to study this phenomenon typically involve estimating the driving force for interfacial mass transfer based on Sherwood number (*Sh*) correlations and the bulk concentration of dissolved gas. This is often not practical since the bulk concentration is often unknown and *Sh* correlations are sometimes not available to provide an accurate description of the associated flow fields. With the use of interface-resolved simulations to model these processes, the local distribution of dissolved gas can be obtained by solving for the concentration field. The driving force for interfacial mass transfer can be computed based on *Sh* correlations (which can be adopted for specific flows and are typically used in "engineering" applications) or the universally applicable Fick's first law. This paper compares the predictions of these approaches for the well-studied case of a two-dimensional bubble growing in an unbounded supersaturated solution for three different levels of supersaturation. The equivalent two-dimensional simulations are run in a previously developed volume of fluid framework on OpenFOAM® [K. J. Vachaparambil and K. E. Einarsrud, Appl. Math. Model. **81**, 690–710 (2020)]. The results show that the choice of an appropriate *Sh* correlation can provide a reasonable estimate of bubble growth. In a more universal approach, which is relevant when the flow being simulated cannot be captured by a single *Sh* correlation (e.g., bubble growth/coalescence and detachment) or when existing *Sh* correlations are not applicable, Fick's first law can be used to compute the driving force for bubble growth, provided that the concentration boundary layer can be resolved.

I. INTRODUCTION

Bubble evolution in supersaturated solutions is a process initiated by nucleation, followed by interfacial mass transfer driven growth and eventually detachment from the surface.[1] This phenomenon is relevant to processes such as electrolysis of water and electrolytic reduction of alumina, as well as to the opening of champagne bottles. As the presence of bubbles reduces the efficiency of electrochemical systems,[2] it is important to efficiently remove them. The bubble growth can be divided into two main regimes: inertial (which lasts for less than a second for very small bubbles of the order of tens of micrometers in size) and diffusion-controlled (the interfacial mass transfer driven regime relevant for continuum scale bubbles).[2] Apart from these two regimes, in electrochemical systems, the heterogeneous reactions that result in supersaturation of the liquid can also affect the bubble growth.[2] Consequently, the continuum-scale bubble growth driven by interfacial mass transfer in supersaturated solutions is an important topic that has been investigated using analytical, numerical, and experimental approaches.

Seminal analytical studies were carried out by Epstein and Plesset[11] and by Scriven[7] in the 1950s. Epstein and Plesset[11] derived an approximate solution for the temporal changes in bubble size starting from a pre-existing bubble, although they neglected the effect of convection induced by the bubble growth. The effect of convection induced by the radially symmetric bubble growth was subsequently treated by Scriven[7] who derived an asymptotic solution describing the bubble growth controlled by interfacial mass transfer. Bruman and Jameson[8] derived a Sherwood number (*Sh*) correlation (see

TABLE I. Some examples of Sherwood number (*Sh*) correlations reported in the literature.

Sh correlation	Applicable flow scenario	References
$Sh = 2$	$Re = 0$ flow around a spherical bubble	3
$Sh = 2 + 0.6515(Re\,Sc)^{1/2}$	$Re \ll 1$ flow around a bubble	4
$Sh = 2 + 0.6Re^{1/2}Sc^{1/3}$	$2 < Re < 200$ flow around a droplet	5 and 6
$Sh = 4\beta^2/\mathfrak{A}$[a]	Bubble growth based on the work of Scriven[7]	8
$Sh = 0.332Re^{1/2}Sc^{1/3}$	Laminar flow over a flat plate	9
$Sh = 1.26Re^{1/3}Sc^{1/3}$	Rising bubble in champagne	10

[a]β and $\mathfrak{A}$ are dimensionless numbers that are defined in Eqs. (16) and (17), respectively.

Table I) based on the bubble growth scenario described by Scriven. The growth of rising bubbles in champagne was also described using a *Sh* correlation by Liger-Belair *et al.*[10] In these works based on *Sh* correlations, the analytical driving force (j_a) for interfacial mass transfer is computed as

$$j_a = M\frac{D\,Sh}{L}(C_\infty - C_{\text{sat}}), \tag{1}$$

where M and D are the molar mass and the diffusion coefficient of the dissolved gas, respectively, L is a characteristic length scale, and $C_\infty - C_{\text{sat}}$ is the difference between the concentration of dissolved gas in the bulk and at the interface (which is assumed to be at saturation). The supersaturation is represented by S, which is calculated as C_∞/C_{sat}. Additionally, these analytical models assume that the bubbles are present in the bulk and are surrounded by an unbounded uniformly supersaturated solution.

In contrast to these analytical models, which present a greatly simplified view of the process, experimental studies have revealed the complex nature of bubble growth, including its dependence on surface wettability and the inhomogeneous distribution of supersaturation around the bubble.[2] Owing to the inhomogeneous distribution of supersaturation, as a result of convection or heterogeneous reactions, the driving force for interfacial mass transfer must be computed based on the local value of the dissolved gas concentration near the interface.

Numerical approaches, especially interface-resolved multiphase models such as the Volume of Fluid (VOF) method, can provide an adequate framework to resolve and study the growth of individual bubbles as well as to solve for the dissolved gas transport to determine its distribution and even treat heterogeneous reactions. However, owing to the difficulty in modeling transport of dissolved gas in multiphase flows and coupling this to the bubble growth, advances in numerical modeling of the latter phenomenon have been made only relatively recently. The transport of dissolved gas in multiphase flows requires treatment of the interface conditions that account for the jump in concentration and that of the continuity of the diffusive fluxes that accounts for interfacial mass transfer.[12] The ways in which these interfacial conditions have been addressed in the literature can be broadly grouped as follows:

- two-field approaches,[12–14] which use individual transport equations for the dissolved species in each phase and in which interfacial conditions are applied as boundary conditions for each phase; and
- single-field approaches,[15–17] which use a single governing equation (which accounts for the interfacial conditions) to describe the transport of dissolved gas in both phases.

Although interfacial mass transfer can be simulated by both types of approaches, the two-field approach has a greater computational requirement owing to the larger number of governing equations that have to be solved, as well as the requirement for the sharp representation of the interface (obtained using geometrical reconstruction in VOF methods).[15] This information about the local concentration of the dissolved gas can be used to obtain a driving force for the interfacial mass transfer and bubble growth, which is computed in one of the following ways:

- Fick's first law provides an accurate representation of interfacial mass transfer for any given flow scenario, but it is computationally expensive owing to the need to resolve concentration gradients at the interface.
- The use of Sherwood number correlations is computationally cheaper and circumvents the need for gradient calculations by means of flow-specific approximations for "engineering" applications. As a result of these approximations, *Sh* correlations can be adopted for specific flow scenarios (see Table I) and can be generally expressed as $Sh = 2 + aRe^bSc^c$, where a, b, and c are case-specific constants, Re is the Reynolds number (the ratio of inertial to viscous forces), and Sc is the Schmidt number (the ratio of the kinematic viscosity to the diffusion coefficient).[16] The associated driving force is computed based on the *Sh* correlations and the local concentration of the dissolved gas near the interface.

A summary of studies that have implemented these methods for determining driving forces and have simulated bubble growth by interfacial mass transfer is presented in Table II. Although the use of a driving force based on Fick's first law provides an accurate and generic representation of bubble growth for any flow scenario, *Sh* correlations are typically used for engineering applications.

The aim of this paper is to compare the bubble growth predictions using driving forces based on Fick's first law and two *Sh* correlations for a bubble growing in an unbounded solution that is supersaturated for a range of values. These driving forces are implemented in a VOF-based framework on OpenFOAM® 6 proposed in our recent work.[21] This flow scenario, which has been thoroughly investigated analytically, is chosen because of the availability of the exact solutions that can be used for the verification of the computational model. The results from the simulations show that carefully chosen *Sh* correlations can provide reasonably predictions that match analytical models. For flow scenarios that cannot be described by a single *Sh* correlation, such as bubble evolution (which includes growth, coalescence, and detachment), Fick's first law should be used to compute the driving force for interfacial mass transfer. Finally, when

TABLE II. Summary of the literature on bubble evolution driven by interfacial mass transfer.

Reference	Interfacial mass transfer	Transport	Concentration treated[a]	VOF scheme[b]
19	*Sh* correlation	Two-field	L[c]	Geometric
20	Fick's first law	Two-field	L + I + G	Geometric
21	Fick's first law	Single-field	L + I	Algebraic
22	Fick's first law	Single-field	L + I + G	Algebraic

[a]This refers to the regions to which the dissolved gas transport model applies: the liquid phase (L), the interfacial region where the jump conditions are treated (I), and the gas phase (G).
[b]Geometric VOF methods employ interface reconstruction within each cell, whereas algebraic VOF methods, which are computationally cheaper, generate an interface based on algebraic techniques (e.g., interface compression), which results in the interface being smeared over a few computational cells.[18]
[c]Interface jump conditions are not described in Ref. 19.

Fick's first law is used, the concentration boundary layer must always be resolved. This paper shows that using the appropriate *Sh* correlation can provide reliable results, which is beneficial for obtaining computationally cheaper simulations in engineering applications. As the effect of gravity has been studied in our previous work,[21] it will not be investigated again here. This paper will also ignore surface tension, since its modeling can lead to the well-known problem of spurious velocities,[18,23–25] which has been reported to alter interface mass transfer.[21]

II. GOVERNING EQUATIONS AND SOLUTION ALGORITHM

The solver used in the this paper, proposed in Ref. 21, is based on the algebraic VOF method used by OpenFOAM® 6 (in the interFoam solver[18]) along with a single-field dissolved gas transport model [the Compressive-Continuous Species Transfer (C-CST) model[17]] and a continuum field representation of source terms that was adapted based on the work of Hardt and Wondra[26] and Kunkelmann.[27] An overview of the governing equation and the overall solution algorithm of the solver is provided in this section; for further details and the derivation of the governing equations, see Ref. 21.

The first step of the solver is advection of the volume fraction of liquid. The volume fraction of liquid, denoted by α_1, is a scalar used in the VOF method to distinguish between the phases. $\alpha_1 = 1$ indicates the liquid (phase 1), $\alpha_1 = 0$ indicates the gas/bubble (phase 2), and $0 < \alpha_1 < 1$ indicates the interfacial region. To preserve the sharpness of the interface, α_1 is advected using the interface compression method (which belongs to the algebraic VOF approach), which is described as follows:

$$\frac{\partial \alpha_1}{\partial t} + \nabla \cdot (\alpha_1 \vec{U}) + \nabla \cdot [\alpha_1 (1 - \alpha_1) \vec{U}_r] = \alpha_1 \nabla \cdot \vec{U}, \tag{2}$$

where the first two terms on the left-hand side are the temporal and convection terms, while the third term, which is nonzero only in the interfacial region, compresses the interface depending on the relative velocity between the phases, $\vec{U}_r$.[18] The term on the right-hand side is associated with the source term that results in the bubble growth.[21] Equation (2) is solved using the semi-implicit multidimensional limiter for explicit solution (MULES) to ensure that α_1 remains bounded.[28] The volume fraction of phase 2, α_2, is calculated as $1 - \alpha_1$. The fluid properties such as density ρ and viscosity ν are computed using volume fraction based algebraic averaging as $\chi = \alpha_1 \chi_1 + \alpha_2 \chi_2$, where $\chi \in [\rho, \nu]$.

Once α_1 has been advected, the driving force for interfacial mass transfer is calculated. The solver computes the transport only to the dissolved gas (see Table II) and determines only the concentration C_i above the saturation condition. These simplifications allow the saturation concentration on the gas side of the interface to be described as 0 mol/m^3, and correspondingly, the driving force can be computed based on one of the following approaches:

- Fick's first law in the form

$$j = M_i D_{i,1} |\nabla C_i|, \tag{3}$$

  where M_i is the molar mass of dissolved gas (i) and $D_{i,1}$ is the diffusion coefficient of the dissolved gas in the liquid. Equation (3) is based on the assumption that the gradient of concentration of the dissolved gas at the interface in the tangential direction is negligible in comparison with the normal component, as discussed by Deising *et al.*[15]
- *Sh* correlation 1: $Sh = 2 + 0.6515\sqrt{Re\,Sc}$, which is applicable for low solubility/small mass transfer rates from the interface to liquid for a bubble in a creeping flow.[4] In this case,

$$j = M_i k_{Sh1} C_i, \tag{4}$$

  with k_{Sh1} given by

$$k_{Sh1} = \frac{D_{i,1}}{2R} Sh = \frac{D_{i,1}}{2R}\left(2 + 0.6515\sqrt{Re\,Sc}\right), \tag{5}$$

  where R is the bubble radius, Re is given by $2RU_\infty/\nu_1$ (where U_∞ is computed as the rate of increase in the bubble radius), and $Sc = \nu_1/D_{i,1}$.
- *Sh* correlation 2: $Sh = 4\beta^2\rho_2/(M_i C_i)$, which is applicable for the bubble growth driven by supersaturation (derived in Appendix A). In this case,

$$\begin{aligned} j = M_i k_{Sh2} C_1 &= \left(\frac{D_{i,1}}{2R}\frac{4\beta^2\rho_2}{M_i C_i}\right) M_i C_i \\ &= 4\beta^2 \rho_2 \frac{D_{i,1}}{2R}, \end{aligned} \tag{6}$$

  where β is the growth coefficient used in Scriven's model[7] and is estimated using Eq. (16).

Based on j, the local mass transfer rate is computed at the liquid side of the interface as

$$\psi_0 = Nj\alpha_1|\nabla\alpha_1|, \tag{7}$$

where N is a normalization factor calculated as $\int_\Omega |\nabla\alpha_1|\,dV / \int_\Omega \alpha_1|\nabla\alpha_1|\,dV$. To improve numerical robustness, the calculated local mass transfer rate is smeared at the interface, according to the method of Hardt and Wondra,[26] using a user-defined value $D\Delta t$ as follows:

$$D\Delta t\nabla^2\psi = \psi - \psi_0. \tag{8}$$

For the simulations reported in this paper, $D\Delta t$ is set equal to 10^{-6} m^2 based on the parametric study reported in our previous work.[21] For numerical stability, the source term for the continuity equation, which is redistributed in the region where $\alpha_1 < 10^{-3}$ using a Heaviside function (as described by Kunkelmann[27]), is expressed as

$$\dot{m} = A\alpha_2\psi, \tag{9}$$

where A is a normalization factor equal to $\int_\Omega \psi_0\,dV / \int_\Omega \alpha_2\psi\,dV$. The sink term in the transport of the dissolved gas is computed at the liquid side of the interface as

$$S_i = -\frac{N\alpha_1(j|\nabla\alpha_1|)}{M_i}, \tag{10}$$

where N is the normalization factor used in Eq. (7).

The momentum equation, using a modified pressure ($p_{\text{rgh}} = p - \rho\vec{g}\cdot\vec{x}$) and a single-field velocity field ($\vec{U}$), is written as

$$\frac{\partial\rho\vec{U}}{\partial t} + \nabla\cdot(\rho\vec{U}\vec{U}) = -\nabla p_{\text{rgh}} + \nabla\cdot(\mu\nabla\vec{U}) + \nabla\vec{U}\cdot\nabla\mu - \vec{g}\cdot\vec{x}\,\nabla\rho + \vec{F}_{\text{ST}}, \tag{11}$$

where $\nabla\cdot(\mu\nabla\vec{U}) + \nabla\vec{U}\cdot\nabla\mu$ are the viscous terms of the momentum equation.[18] As the surface tension effects are not simulated in this paper, $\vec{F}_{\text{ST}}$, which is the volumetric surface tension force, will not be considered here. As the densities of the individual phases are assumed to be constant, mass conservation can be described using the continuity equation as

$$\nabla\cdot\vec{U} = \frac{\dot{m}}{\rho}, \tag{12}$$

where $\dot{m}$ is the source term for phase 2 computed in Eq. (9). The momentum and continuity equations are solved together using the pressure implicit with splitting of operator (PISO) algorithm.[18,21]

Finally, the C-CST model[17] for the transport of the dissolved gas is solved,

$$\frac{\partial C_i}{\partial t} + \nabla\cdot(\vec{U}C_i) = \nabla\cdot(\hat{D}_i\nabla C_i) - \nabla\cdot\left(\hat{D}_i\frac{1-He_i}{\alpha_1+\alpha_2He_i}C_i\nabla\alpha_1\right) - \nabla\cdot\left(\frac{1-He_i}{\alpha_1+\alpha_2He_i}\alpha_1\alpha_2\vec{U}_rC_i\right) + S_i, \tag{13}$$

where S_i is computed using Eq. (10), He_i describes the interfacial jump in concentration, which is set to 10^{-4} to reliably model just the dissolved gas,[21] $\vec{U}_r$ is the relative velocity between the phases that appears in Eq. (2), and $\hat{D}_i$ is the harmonic average of the diffusion coefficients of the phases.[17]

TABLE III. Settings used to solve the governing equations.

Equation	Linear solver	Smoother/preconditioner	Tolerance
p_{rgh}	PCG	GAMG	10^{-20}
$\vec{U}$	smoothSolver	symGaussSeidel	10^{-10}
α_1	smoothSolver	symGaussSeidel	10^{-10}
C_i	PBiCGStab	Diagonal	10^{-10}
ψ	PCG	DIC	10^{-10}

A. Numerical settings

The governing equations are discretized with the first- and second-order schemes in time and space,[21] respectively, and computed using the iterative solvers listed in Table III. Other OpenFOAM® specific numerical settings, such as MULESCorr and momentumPredictor, are set as described in our previous work.[21] The maximum time step is set by applying an upper limit on the Courant number equal to 0.05. The iterative solver used to solve for ψ, given in Table III, is used instead of the settings used in our previous work,[21] namely, PBiCGStab–diagonal, to reduce the computational time required, as described in Appendix B.

III. RESULTS AND DISCUSSION

A. Problem description

The computational domain and boundary/initial conditions used in the simulations are presented in Fig. 1. The fluid properties used in the simulations, adapted from our previous work,[21] are listed in Table IV. The supersaturation levels used in the simulations

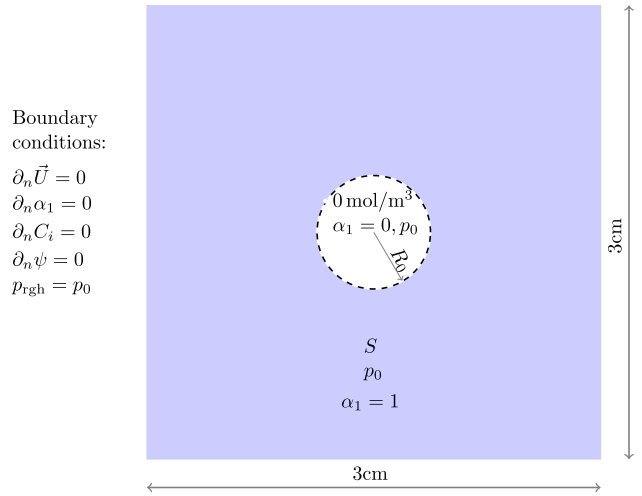

FIG. 1. Computational domain and boundary/initial conditions used in the simulations. The operating pressure (p_0) and the pre-existing bubble radius (R_0) used in the simulations are equal to 101 325 Pa and 250 μm, respectively. The concentration of the dissolved gas at $t = 0$ s is set based on the various levels of supersaturation S.

TABLE IV. Fluid properties used for the simulations (adapted from Ref. 21).

Property	Phase 1 (liquid)	Phase 2 (bubble)
Density (kg/m^3)	997.0751 (Ref. 29)	1.81 (Ref. 30)
Viscosity (m^2/s)	8.92×10^{-7} (Ref. 29)	8.228×10^{-6} (Ref. 30)
Diffusion coefficient (m^2/s)	1.94×10^{-9} (Ref. 31)	9.18×10^{-6} (Ref. 32)
Molar mass (kg/mol)	44×10^{-3} (Ref. 21)	

are 2.5, 4, and 7, which correspond to the initialized concentrations of dissolved gas C_i equal to 50.16 mol/m^3, 100.32 mol/m^3, and 200.64 mol/m^3, respectively (with a saturation concentration equal to 33.44 mol/m^3). It should be noted that the initialized uniform distribution of the dissolved gas does not take account of any concentration boundary layer, the implications of which will be explored later in the discussion of the results. Again, both surface tension and gravity are neglected in the simulations, but we have investigated the influence of these parameters on growth previously.[21] The mesh used for all the simulations presented in this paper had a uniform hexahedral grid of 16×10^6 cells based on grid convergence studies performed for the bubble growth associated with $S = 7$ and a driving force based on Fick's first law in our previous work.[21]

B. Choice of analytical model

As the Epstein–Plesset model[11] ignores the effect of bubble growth on interfacial mass transfer, Scriven's asymptotic solution[7] provides the most reliable description of bubble growth via interfacial mass transfer, as was also noted by Burman and Jameson.[8] According to Scriven,[7] the increase in bubble radius can be described as

$$R_{\text{Scriven}} = 2\beta\sqrt{D_{i,1}t}, \tag{14}$$

where β is the growth coefficient. To treat the interfacial mass transfer driven growth of a pre-existing bubble, Scriven's solution was extended by Hashemi and Abedi[33] (in what we will refer to here as the "extended Scriven model") where the evolution of the bubble radius is described by

$$R_{\text{Scriven-ext}} = 2\beta\sqrt{D_{i,1}\left(t + \frac{R_0^2}{4D_{i,1}\beta^2}\right)}, \tag{15}$$

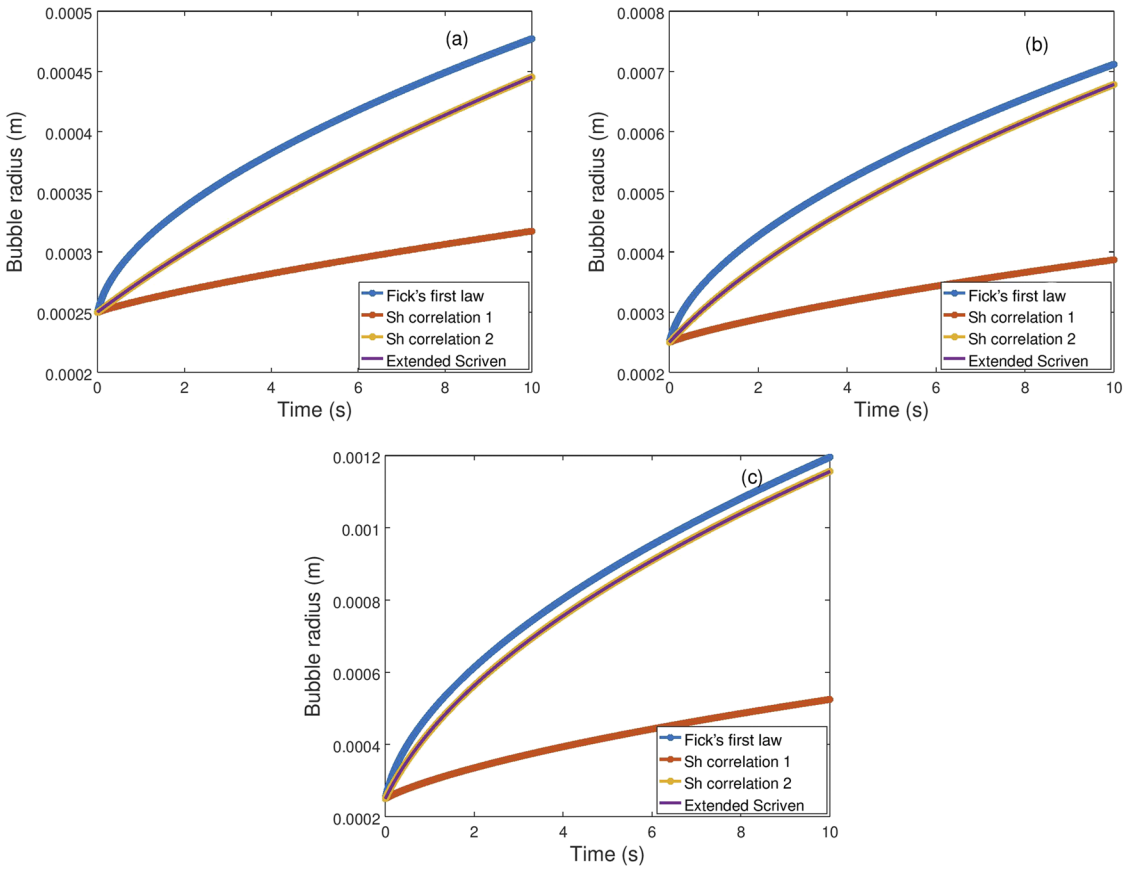

FIG. 2. Comparison of the results of simulations of bubble radius evolution using the driving forces based on Fick's first law [Eq. (3)] and on *Sh* correlations [Eqs. (4) and (6)] with the results of the extended Scriven model (with β_{2D}) for various levels of supersaturation: (a) 2.5, (b) 4.0, and (c) 7.0.

where R_0 is the radius of the pre-existing bubble. Our previous work[21] has shown that Eq. (15) provides a better representation of the process of interfacial mass transfer driven bubble growth from a pre-existing bubble when compared to Eq. (14).

The growth coefficient for two-dimensional bubbles should be calculated as[21]

$$\beta_{2D} = \frac{\mathfrak{A} + \sqrt{\mathfrak{A}^2 + 4\mathfrak{A}}}{2\sqrt{2}}, \tag{16}$$

where $\mathfrak{A}$ is calculated as

$$\mathfrak{A} = \frac{M_i \Delta C}{\rho_2}, \tag{17}$$

with ΔC being the concentration of the dissolved gas in the bulk above the saturation condition. As the simulations in this paper deal with the growth of a two-dimensional bubble from a pre-existing bubble, the theoretical model used to verify the simulations is the extended Scriven model [Eq. (15)] with the growth coefficient determined based on Eq. (16). As ΔC in the simulations is set to 50.16 mol/m^3, 100.32 mol/m^3, and 200.64 mol/m^3, the corresponding values of β_{2D} are 1.3230, 2.2632, and 4.0509, respectively.

C. Verification of the simulations

As the simulations predict bubble growth due to uniform supersaturation, the velocity and concentration of the dissolved gas around the bubble are radially symmetric (as reported in our previous work[21]). Figure 2 compares the increase in bubble radius predicted by simulations using a driving force for interfacial mass transfer based on Fick's first law and on *Sh* correlations with the prediction by the analytical solution of the extended Scriven model for various supersaturation levels. The simulations using a driving force based on *Sh* correlation 1 underpredict the bubble size compared with the analytical model for all three supersaturation levels. Interestingly, the simulation using a driving force based on Fick's first law appears to agree with the analytical model at larger supersaturation, whereas the simulations using a driving force based on *Sh* correlation 2 exhibits good agreement with the extended Scriven model for all three supersaturation levels.

As the interfacial mass transfer is proportional to the surface area of the bubble (which in the case of a two-dimensional bubble is proportional to the bubble radius), a normalized growth rate based on the bubble radius, which is computed as $\int \psi_0 dV/R$, is used to account for the different bubble sizes.[21] In the extended

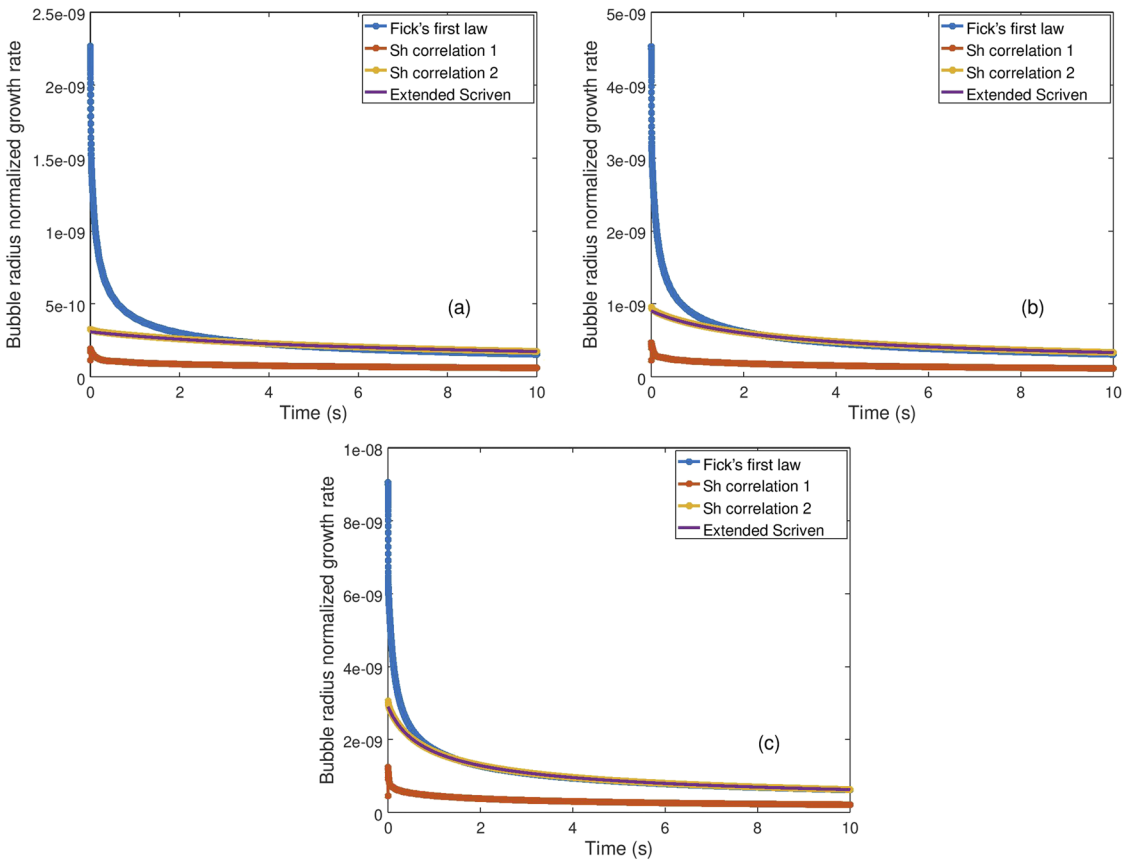

FIG. 3. Comparison of the results of simulations of bubble radius normalized growth rates (kg m^{-1} s^{-1}) based on Fick's first law [Eq. (3)] or on *Sh* correlations [Eqs. (4) and (6)] with the results of the extended Scriven model (with β_{2D}) for various levels of supersaturation: (a) 2.5, (b) 4.0, and (c) 7.0.

Scriven model, the radius normalized growth rate is computed as the rate of change in the mass of the bubble divided by the bubble radius based on the analytical model, i.e., Eq. (15). The discrepancies between the temporal change in bubble radius computed using a driving force based on Fick's first law or on *Sh* correlations and that computed using the analytical extended Scriven model can be explained based on the bubble radius normalized growth rate (see Fig. 3). The driving force based on *Sh* correlation 1 used for the simulations appears to underpredict the radius normalized growth rate (see Fig. 3) compared with the analytical model, which results in the bubble being smaller (see Fig. 2). On the other hand, the evolution of the bubble radius predicted using a driving force based on *Sh* correlation 2 agrees reasonably well with the analytical model, since the normalized growth rates from the two methods match, with an absolute deviation of less than 1% for all three cases at $t = 10$ s (see Figs. 2 and 3). As the initialized distribution of the dissolved gas does not take account of the concentration boundary layer, the local value of C_i, which is used to calculate j based on Eq. (4), is close to the bulk supersaturation, which causes the initial spike in the normalized growth rate observed in Fig. 3. As the simulation proceeds over time, a concentration boundary layer develops, and the local C_i becomes lower than the bulk supersaturation. Although for *Sh* correlations, j is calculated to be proportional to C_i, Fick's first law computes j based on the gradient of the local concentration [see Eq. (3)]. As a result of this gradient-based calculation, the use of j from Fick's first law leads to a large normalized growth rate that is greater than the analytical solution, as observed in Fig. 3. As the concentration boundary layer becomes fully developed, the simulated radius normalized growth rate matches the analytical solution for all three supersaturation levels. This initial larger growth rate in the simulations causes the bubble radius to increase more rapidly than expected, which results in the discrepancy observed in Fig. 2.

IV. CONCLUSIONS

In this paper, the VOF-based approach proposed previously[21] has been used to simulate the interfacial mass transfer driven growth of a bubble in a unbounded and uniformly supersaturated solution (for $S = 2.5$, 4, and 7). As an analytical solution is available for this flow scenario, the results of simulations with the driving forces computed based on Fick's first law and on two *Sh* correlations have been compared with the theoretical results to assess the predictions of bubble growth. The results reveal the following:

- If a *Sh* correlation that is appropriate for the specific flow being simulated is chosen to compute the driving force for interfacial mass transfer, a reasonably accurate prediction of bubble growth can be obtained. In the case of radially symmetric bubble growth driven by supersaturation, *Sh* correlation 2 [Eq. (6)] is better suited than *Sh* correlation 1 [Eq. (4)].
- If *Sh* correlations are not available to describe a flow scenario or if a single correlation cannot capture a complex phenomenon (such as bubble growth, coalescence, and detachment), the driving force should be computed based on Fick's first law, since it provides a better representation of the flow than a single *Sh* correlation with limited applicability.
- The driving force computed using Fick's first law has been shown to be able to handle bubble growth for a range of supersaturation levels, provided that the concentration boundary layer has been resolved, even at $t = 0$ s.
- The driving forces based on *Sh* correlations and Fick's first law are proportional to the local concentration and the gradient of C_i. This means that the computational requirements (with respect to mesh resolution) needed with *Sh* correlations are lower than when Fick's first law is used, since the latter requires the resolution of concentration gradients near the interface.

Future work within this framework will utilize a driving force computed based on the local concentration to model the bubble growth driven by heterogeneous reactions such as electrochemical gas evolution.

ACKNOWLEDGMENTS

This work was funded by the Department of Materials Science and Engineering at NTNU, and the required computational resources were provided by UNINETT Sigma2 through Grant NN9741K.

APPENDIX A: DERIVATION OF *Sh* CORRELATION 2

In this appendix, based on the original work by Burman and Jameson,[8] we extend their approach to derive *Sh* correlation that is used in simulations.

For a two-dimensional bubble as simulated in this paper, the growth rate can be expressed as

$$\rho_2 \frac{dV}{dt} = jA, \tag{A1}$$

where $V = \pi R^2 h$, $A = 2\pi R h$, and $j = M_i k C_i$, with h being the unit cell thickness used to define the two-dimensional domains in OpenFOAM®, which in this paper is set to 1 μm. Substituting the expressions for V, A, and j, we get

$$\rho_2 \frac{dR}{dt} = M_i k C_i. \tag{A2}$$

The rate of change in the radius can be calculated based on Eq. (15) as

$$\frac{dR}{dt} = \frac{2\beta^2 D_{i,1}}{R}. \tag{A3}$$

Substituting Eq. (A3) into Eq. (A2), we get

$$\frac{2\beta^2 D_{i,1}}{R} = \frac{M_i k C_i}{\rho_2}. \tag{A4}$$

This equation can be rearranged and multiplied by 2 on both sides to give

$$k = \frac{D_{i,1}}{2R} \frac{4\beta^2 \rho_2}{M_i C_i}, \tag{A5}$$

and the corresponding *Sh* is defined as $4\beta^2 \rho_2 / (M_i C_i)$. In the work by Burman and Jameson,[8] the value of C_i is written in terms of the

bulk concentration of the dissolved gas under the assumption of diffusion-limited mass transfer through the liquid film. This leads to Sh being defined as $4\beta^2\rho_2/(M_i\Delta C)$, where ΔC is defined as in Eq. (17). At a very low supersaturation, when Re is approximately zero and β is small, Burman and Jameson[8] showed that $Sh \to 2$, as expected for the case of diffusive mass transfer in the absence of convection (see Table I).

APPENDIX B: CHOICE OF LINEAR SOLVER AND PRECONDITIONER

To reduce the computational time required for the simulations, the effect of the iterative solver used to smear ψ_0 [Eq. (8)], which is the bottleneck in the simulation at each time step, is investigated in this appendix. Bubble growth driven by supersaturation $S = 7$ is chosen as the flow scenario to be simulated, with the convergence criterion for Eq. (8) set at 10^{-10}. The first case corresponds to the setting used in this paper, i.e., Eq. (8) is solved using PCG (linear solver)–DIC (preconditioner). The second case corresponds to the setting used in our previous work,[21] i.e., Eq. (8) is solved using PBiCGStab (linear solver)–diagonal (preconditioner).

Although the bubble growths predicted by the two simulations are in very close agreement (see Fig. 4), the number of iterations required for the convergence of Eq. (8) is reduced by almost half at every time step, as observed in the log file obtained from the solver during the run:

- For the PCG–DIC solver setting:
  - At $t = 0$ s:DICPCG: Solving for psi, Initial residual = 1, Final residual = 9.88185e − 11, No Iterations 1842
  - At $t = 10$ s:DICPCG: Solving for psi, Initial residual = 0.0132484, Final residual = 9.94304e−11, No Iterations 1218
- For the PBiCGStab–diagonal solver setting:
  - At $t = 0$ s:diagonalPBiCGStab: Solving for psi, Initial residual = 1, Final residual = 4.55196e−11, No Iterations 4020
  - At $t = 10$ s:diagonalPBiCGStab: Solving for psi, Initial residual = 0.0131794, Final residual = 9.72418e−11, No Iterations 2904

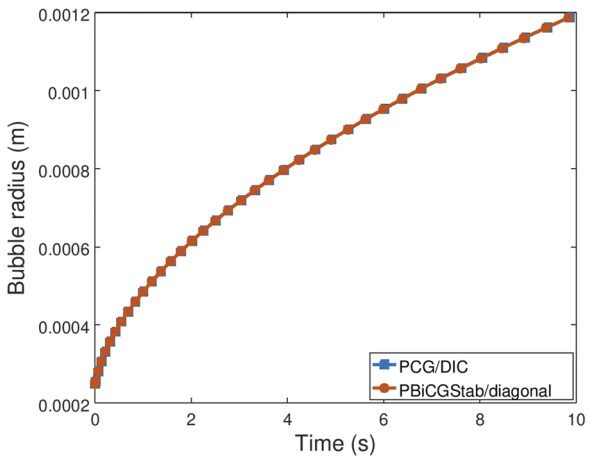

FIG. 4. Bubble size simulated using the various solvers for Eq. (8). The bubble evolution for the PBiCGStab/diagonal setting is obtained from the data reported in our previous work.[21]

DATA AVAILABILITY

The data that support the findings of this study are available within the article.

REFERENCES

[1]S. Jones, G. Evans, and K. Galvin, "Bubble nucleation from gas cavities—A review," Adv. Colloid Interface Sci. **80**, 27–50 (1999).
[2]G. Sakuma, Y. Fukunaka, and H. Matsushima, "Nucleation and growth of electrolytic gas bubbles under microgravity," Int. J. Hydrogen Energy **39**, 7638–7645 (2014).
[3]J. Villadsen, J. Nielsen, and G. Lidén, *Bioreaction Engineering Principles* (Springer, 2011).
[4]R. Bird, W. Stewart, and E. Lightfoot, *Transport Phenomena* (Wiley, 2006).
[5]W. E. Ranz and W. R. Marshall, "Evaporation from drops," Chem. Eng. Prog. **48**, 141–146 (1952), available at http://dns2.asia.edu.tw/~ysho/YSHO-English/1000%20CE/PDF/Che%20Eng%20Pro48,%20141.pdf.
[6]C. Crowe, J. Schwarzkopf, M. Sommerfeld, and Y. Tsuji, *Multiphase Flows with Droplets and Particles* (CRC Press, 2011).
[7]L. E. Scriven, "On the dynamics of phase growth," Chem. Eng. Sci. **10**, 1–13 (1959).
[8]J. Burman and G. Jameson, "Diffusional mass transfer to a growing bubble," Chem. Eng. Sci. **31**, 401–403 (1976).
[9]G. Brenn, "Mass transfer," in *Analytical Solutions for Transport Processes: Fluid Mechanics, Heat and Mass Transfer* (Springer, 2017), pp. 239–270.
[10]G. Liger-Belair, M. Vignes-Adler, C. Voisin, B. Robillard, and P. Jeandet, "Kinetics of gas discharging in a glass of champagne: The role of nucleation sites," Langmuir **18**, 1294–1301 (2002).
[11]P. S. Epstein and M. S. Plesset, "On the stability of gas bubbles in liquid–gas solutions," J. Chem. Phys. **18**, 1505–1509 (1950).
[12]D. Bothe and S. Fleckenstein, "A volume-of-fluid-based method for mass transfer processes at fluid particles," Chem. Eng. Sci. **101**, 283–302 (2013).
[13]P. S. Weber, H. Marschall, and D. Bothe, "Highly accurate two-phase species transfer based on ALE interface tracking," Int. J. Heat Mass Transfer **104**, 759–773 (2017).
[14]M. Falcone and H. Marschall, "Explicit radial-basis-function-based finite-difference method for interfacial mass-transfer problems," Chem. Eng. Technol. **40**, 1385–1390 (2017).
[15]D. Deising, H. Marschall, and D. Bothe, "A unified single-field model framework for volume-of-fluid simulations of interfacial species transfer applied to bubbly flows," Chem. Eng. Sci. **139**, 173–195 (2016).
[16]D. Deising, D. Bothe, and H. Marschall, "Direct numerical simulation of mass transfer in bubbly flows," Comput. Fluids **172**, 524–537 (2018).
[17]J. Maes and C. Soulaine, "A new compressive scheme to simulate species transfer across fluid interfaces using the volume-of-fluid method," Chem. Eng. Sci. **190**, 405–418 (2018).
[18]S. S. Deshpande, L. Anumolu, and M. F. Trujillo, "Evaluating the performance of the two-phase flow solver interFoam," Comput. Sci. Discovery **5**, 014016 (2012).
[19]H. Liu, L.-M. Pan, and J. Wen, "Numerical simulation of hydrogen bubble growth at an electrode surface," Can. J. Chem. Eng. **94**, 192–199 (2016).
[20]S. Fleckenstein and D. Bothe, "A volume-of-fluid-based numerical method for multi-component mass transfer with local volume changes," J. Comput. Phys. **301**, 35–58 (2015).

[21]K. J. Vachaparambil and K. E. Einarsrud, "Numerical simulation of bubble growth in a supersaturated solution," Appl. Math. Modell. **81**, 690–710 (2020).
[22]J. Maes and C. Soulaine, "A unified single-field volume-of-fluid-based formulation for multi-component interfacial transfer with local volume changes," J. Comput. Phys. **402**, 109024 (2020).
[23]J. Klostermann, K. Schaake, and R. Schwarze, "Numerical simulation of a single rising bubble by VOF with surface compression," Int. J. Numer. Methods Fluids **71**, 960–982 (2013).
[24]K. J. Vachaparambil and K. E. Einarsrud, "Comparison of surface tension models for the volume of fluid method," Processes **7**, 542 (2019).
[25]K. J. Vachaparambil and K. E. Einarsrud, "On sharp surface force model: Effect of sharpening coefficient," Exp. Comput. Multiphase Flow (published online 2020).
[26]S. Hardt and F. Wondra, "Evaporation model for interfacial flows based on a continuum-field representation of the source terms," J. Comput. Phys. **227**, 5871–5895 (2008).
[27]C. Kunkelmann, "Numerical modeling and investigation of boiling phenomena," Ph.D. thesis, Technische Universität, Darmstadt, 2011.
[28]C. Greenshields, See https://openfoam.org/release/2-3-0/multiphase/ for Predictor-corrector semi-implicit MULES, 2014; accessed on 17 June 2020.
[29]J. Kestin, M. Sokolov, and W. A. Wakeham, "Viscosity of liquid water in the range −8° C to 150° C," J. Phys. Chem. Ref. Data **7**, 941–948 (1978).
[30]H. Iwasaki and M. Takahashi, "Viscosity of carbon dioxide and ethane," J. Chem. Phys. **74**, 1930–1943 (1981).
[31]A. Tamimi, E. B. Rinker, and O. C. Sandall, "Diffusion coefficients for hydrogen sulfide, carbon dioxide, and nitrous oxide in water over the temperature range 293–368 K," J. Chem. Eng. Data **39**, 330–332 (1994).
[32]E. B. Winn, "The temperature dependence of the self-diffusion coefficients of argon, neon, nitrogen, oxygen, carbon dioxide, and methane," Phys. Rev. **80**, 1024–1027 (1950).
[33]S. J. Hashemi and J. Abedi, "Advances in modeling of new phase growth," Energy Fuels **21**, 2147–2155 (2007).